ACS OMEGA

Open Access

http://pubs.acs.org/journal/acsodf

Article

Exploring the Morphological Effect of Zeolite Beta on Catalytic Cracking of Polyethylene

Jeonghwan Seo, Daeun Kim, and Yong-Kul Lee*

Cite This: *ACS Omega* 2024, 9, 44760−44769

Read Online

ACCESS | Metrics & More | Article Recommendations | Supporting Information

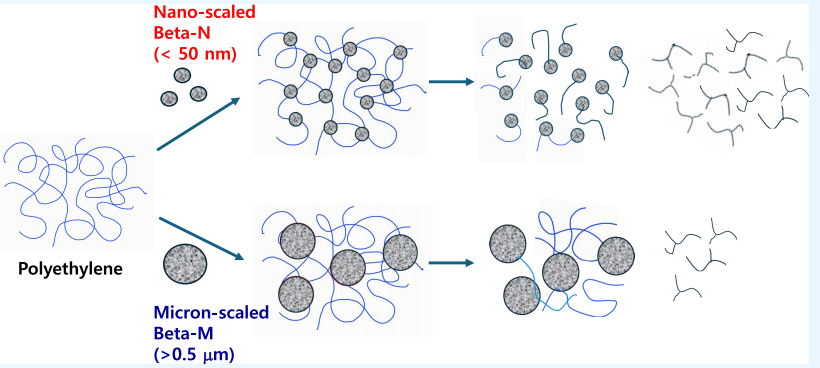

ABSTRACT: Two types of zeolite catalysts, namely, nanosized Beta-N and micrometer-sized Beta-M, were used to crack low-density polyethylene (LDPE) with three different molecular weights: 4000, 200,000, and 3,000,000. The structural and acidic properties were analyzed by N_2 physisorption, transmission electron microscopy, X-ray diffraction, temperature-programmed desorption of isopropylamine (IPA-TPD), and pyridine-adsorbed FTIR. The catalytic activity was tested at 623 K and 3.5 N_2 MPa in an autoclave batch reactor for PE cracking. High Mw PE required higher decomposition activation energy due to transfer limitation. Beta-N showed better activity in PE cracking than Beta-M, with PE conversion of 82.7 and 62.0% for Beta-N and Beta-M, respectively. In addition, the nanosized Beta-N exhibited quite lower activation energy of catalytic PE decomposition than Beta-M, obtained by the Kissinger method in TGA measurement. The characterization results demonstrated that the Beta-N has abundant interparticulate mesopores to provide better dispersion for the catalysts into PE melt and the proximity of the cracking active sites. These results revealed that the Beta-N catalyst shows superior activity for the cracking of polyolefins.

1. INTRODUCTION

Presently, the majority of plastics are not subjected to recycling processes but rather are directed toward incineration and disposal in landfills.[1] If present manufacturing and waste management practices persist, about 12,000 million metric tons (Mt) of plastic garbage will be deposited in landfill sites or the natural environment by 2050, based on a preliminary calculation.[2−4] Hence, immediate measures are necessary to recycle plastic garbage. Regarding plastic garbage, about 60% of the total plastic in municipal solid waste is made up of polyolefins, specifically polypropylene (PP) and polyethylene (PE). Polyethylene (PE) has a global yearly output exceeding 100 million metric tons. Since the PE is composed of robust C−C and C−H bonds, it exhibits remarkable resistance to oxidation,[5] which necessitates a significant amount of energy. The process of depolymerization in PE is thermodynamically difficult. In addition, the usual depolymerization processes are also accompanied by secondary reactions and undesired byproducts, ultimately leading to a decrease in recycling efficiency.[6] Lately, chemical recycling (CR) has emerged as a promising solution to address the aforementioned limitations.[7,8] PE depolymerization can be achieved using thermal, catalytic, or hydrocracking methods.[9] Thermal cracking is carried out at temperatures usually above 500 °C, resulting in a significant energy consumption.[10] The product composition is intricate as a result of the radical processes included in the cracking process.[11] Catalytic cracking employs a protolytic cracking process, enabling the utilization of significantly lower temperatures compared to thermal cracking.[12]

Highly acidic catalysts are employed in the catalytic cracking process of polyolefins to generate alkylbenzene and gaseous hydrocarbons by end-cracking, aromatization, and dehydrogenation. Conversely, acid catalysts with moderate strength produce liquid fractions by random-chain breaking.[13] How-

Received: August 21, 2024
Revised: October 7, 2024
Accepted: October 10, 2024
Published: October 22, 2024

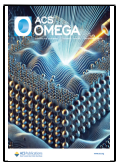

ever, very acidic catalysts also lead to the creation of coke. Therefore, catalysts that are ideal for transforming waste plastics into distillates should have the right level of acidity and a suitable range of pore sizes. Zeolites are crystalline aluminum silicates with a microporous structure. Heterogeneous catalysts and adsorbents for gas separation are often used in many applications.[14] Micropores are characterized by a pore diameter smaller than 2 nm; mesopores have a pore diameter ranging from 2 to 50 nm, and macropores have a pore width of more than 50 nm. Diffusion limitations may occur when the dimensions of the polymer molecules are comparable to or larger than the dimensions of the zeolite crystals.[15] Methods to overcome the constraints of diffusion involve adding a solvent to enhance the rate at which intermediate products (liquid fractions) can diffuse, increasing acid sites, and minimizing excessive cracking.[16] An effective method for accomplishing this is by the utilization of nanoscale zeolite crystals.[17−19] Marcilla et al. conducted a study utilizing TGA and DTG analyses to investigate the breakdown of LDPE using Beta or ZSM-5 zeolites. They found that the zeolite Beta, with its large exterior surface area, resulted in improved performance in the decomposition of PE.[20] Aguado et al. also confirmed the superior activity of zeolite Beta in the cracking of polyolefins.[21] Kokuryo et al. demonstrated that the coke formation in LDPE cracking over zeolite Beta can be resolved by the incorporation of Cr in the zeolite,[22] and they also demonstrated that structural defects of zeolite Beta seem to be effective for the decomposition of LDPE at lower temperatures.[23] Nanosized crystals, the use of so-called embryonic zeolites,[24,25] and so-called hierarchical zeolites[26,27] where meso- and/or macropores are connecting in a topologically arranged network of inter- or intracrystalline structures have been explored to lessen diffusion limitation and improve accessibility to acid sites. More recently, Liu et al. synthesized wide ranges of zeolite Beta series with different levels of acidity and porosity for the PE cracking and revealed that mesoporous zeolites with intermediate acid strength favor the production of gas oils or lubricant base oils, while microporous ones with strong acidity facilitate lighter hydrocarbons via multiple cracking.[28]

While the positive benefits of nanosized zeolites on polymer cracking are well acknowledged, the specific influence of nanoscaled zeolites on polyethylenes of varying molecular weights is not well understood. The catalytic activity is anticipated to vary in line with the polymer's molecular weight level, as its properties are dependent on its molecular weight. This work demonstrates the utilization of thermogravimetry analysis (TGA) to investigate the thermal degradation properties of polyethylenes with different molecular weights. The investigation includes diverse heating rates and the presence or absence of two distinct zeolite Beta catalysts with different structures. Subsequently, the activation energies were determined utilizing the Kissinger model.[29] Furthermore, the catalytic cracking of polyethylene (PE) was carried out in an autoclave batch reactor to examine and evaluate the performance as proven by the TGA. The reaction test revealed the enhanced catalytic efficiency of nanosized zeolite Beta, especially in the cracking of high-molecular-weight polyethylene compared to the micron-sized one. This study offers concrete evidence and a crucial understanding of the design of catalysts to enhance the conversion of plastic waste into useful fuels or chemicals.

2. EXPERIMENTAL SECTION

2.1. Materials. Two types of zeolite Beta catalysts, nanosized Beta (CP814E, Zeolyst) and micrometer-sized Beta (HSZ-931HOA, Tosoh), denoted as Beta-N and Beta-M, respectively, were commercially obtained and calcined at 823 K before use. Low (Mw = 4000), medium (200,000), and high (3,000,000) Mw low-density polyethylenes (LDPE) were purchased from Sigma-Aldrich, Alfa Aesar, and Sigma-Aldrich, respectively.

2.2. Characterization. The X-ray diffraction (XRD) patterns of the zeolite samples were analyzed using a diffractometer (Rigaku DMAX-2500) operating at 60 kV and 300 mA, with Cu Ka radiation (λ = 0.15418 nm). The Scherrer equation was used to calculate the crystallite sizes from the XRD peaks., Dc = $K\lambda/\beta\cos\theta$, where λ represents the wavelength of the X-ray radiation and β is the peak width at half-maximum in radians. K is a constant taken as 0.9 corrected for instrumental broadening (0.1), and 2θ represents the Bragg angle of the reflection. The N_2 physisorption isotherms of the zeolite sample were determined using a Micromeritics ASAP 2010 micropore size analyzer. The specific surface area was determined by the linear section of BET plots (P/P_o = 0.01−0.10) at 77 K. The pore size distribution was calculated by using the BJH method based on the desorption branch of the isotherm. The JEM-2100F 200 kV microscope was used to acquire high-resolution transmission electron microscopy (HR-TEM) pictures. The acidity of the produced zeolites was assessed by using isopropylamine temperature-programmed desorption (IPA-TPD) in a chemisorption device. The catalyst sample, weighing 0.05 g, was placed into a U-tube reactor made of quartz glass. It was then heated gradually at a rate of 7 K/min until it reached a temperature of 673 K. This preheating process lasted for 60 min, while helium gas was flowing through the reactor. After the preheating, the sample was exposed to isopropylamine (IPA) at a temperature of 373 K. The measurement of IPA-TPD was performed in the temperature range of 373−1073 K, with a heating rate of 10 K/min, and under a helium flow rate of 100 cm^3 min^{-1}. A mass spectrometer (HP 5973 inert) monitored the desorbed species in real-time. The recorded signals corresponded to the following molecular ions: m/z = 17 and 15 for NH_3, 18 for H_2O, 44 for IPA, and 41 for propylene. The Fourier transform infrared spectrometer (Frontier IR, PerkinElmer) with an MCT detector and an in situ transmission cell with water-cooled KBr windows was used to capture the infrared spectra of pyridine adsorbed onto the zeolite samples. The samples were compressed into self-supporting wafers 20 mm in diameter and 13 g. The IR spectra were obtained using the absorbance mode with a resolution of 2 cm^{-1}. A total of 64 scans were performed in the range 4000−400 cm^{-1}. An investigation was conducted on these samples to assess the impact of temperature on the acidity of the catalysts. A He flow was used to conduct in situ FTIR measurements on the zeolite samples. The samples underwent pretreatment in a helium flow at a temperature of 673 K for 2 h. The pyridine adsorption measurements were conducted by exposing the samples to a gaseous pyridine flow that was evaporated using a bubbler. The experiment was carried out at a temperature of 373 K and a carrier flow rate of 50 cm^3 min^{-1} helium until saturation was reached. The samples underwent a process of purging with a flow of He for 5 h at a temperature of 373 K to eliminate gaseous pyridine. This was followed by gradually

https://doi.org/10.1021/acsomega.4c07723
ACS Omega 2024, 9, 44760−44769

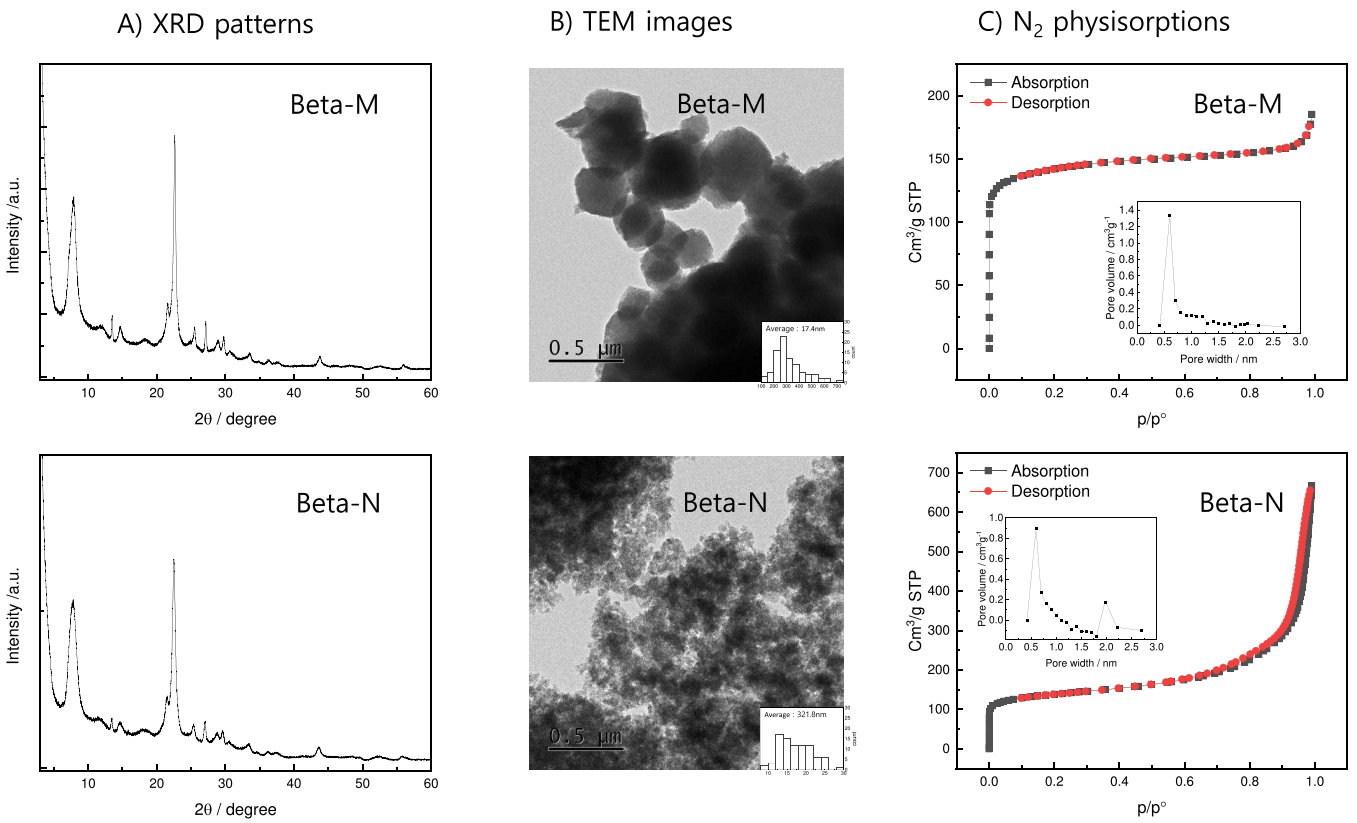

Figure 1. Structural properties of zeolite Beta catalysts: (A) XRD patterns, (B) TEM images, and (C) N_2 physisorption profiles.

increasing the temperature to 423 K to remove pyridine that was only weakly attached to the samples. Measurements were conducted at intervals of 50 K up to a maximum temperature of 673 K.

The TGA analysis was conducted by using a thermogravimetric analyzer (TGA4000, PerkinElmer). The experiment utilized nitrogen gas with a minimum purity of 99.99%. The gas was supplied at a flow rate of 20 cm^3 min^{-1}. The temperature of the sample was monitored by using a thermocouple positioned at the crucible. The polymer utilized for the investigation was a commercially available low-density polyethylene (LDPE) that was blended with varying proportions of the zeolitic catalyst, including different catalyst concentrations ranging from 0 to 40%. The samples were immediately created in the TGA pan by accurately weighing the appropriate quantities of the powdered polymer and catalyst to achieve about 10 mg of a combination. Experiments were conducted under dynamic settings by using three distinct heating rates: 5, 10, 15, 20, and 35 K/min. The mixes vary in catalyst concentration from 0 to 40% (w/w).

2.3. Catalytic Cracking of Polyethylene. The LDPE cracking was conducted in a 120 mL autoclave reactor, as displayed in Figure S1. Initially, 5.0 g of a polyethylene (PE-L) mixture was blended with 0.5 g of catalyst, which had a weight percentage of 10%. Once the mixture was placed into the reactor, nitrogen was introduced at a rate of 50 mL/min to eliminate any air and water vapors. The reactor was subsequently heated to a temperature of 423 K at a heating rate of 5 K min^{-1} and maintained for 1 h to remove moisture that had been adsorbed. After that, the nitrogen feed was discontinued, and in the closed condition, it was heated to the reaction temperature of 623 K at a heating rate of 5 K min^{-1} with a rotation per minute (RPM) of 1000. When the reaction temperature reached 623 K, the reactor pressure became 2.8 MPa in the absence of a catalyst and 3.3 and 3.7 MPa for Beta-M and Beta-N, respectively. In the course of the reaction for 2 h, the pressures increased by 0.3, 0.2, and 0.1 MPa for each reaction. To quantify the product by phase, the reaction products were dissolved in hexane followed by centrifugation, and the residual precipitate was then dried at 353 K in the oven to remove the remaining liquid product. The residue represents the catalyst, and unconverted PE and the products were categorized into three distinct groups: gases, liquid hydrocarbons, and precipitates. The quantity of gaseous products was determined by subtracting the mass of liquid products and residues from the initial mixture. The liquid products were analyzed by using GC-FID and GC-MS for both quantitative and qualitative evaluations.

3. RESULTS AND DISCUSSION

3.1. Structure and Acidity of Zeolite Beta. The structural properties of the zeolite Beta samples, including XRD patterns, TEM images, and N_2 physisorption, were demonstrated, as shown in Figure 1. It is evident that Beta-M exhibits a stronger peak intensity than Beta-N, indicating higher crystallinity for Beta-M. TEM images also support the XRD results, showing the presence of bigger particles of 0.1−1.0 μm for Beta-M and smaller particles of 10−50 nm for Beta-N. N_2 physisorption profiles of the zeolite Beta catalysts are also shown in Figure 1C. Generally, microporous materials exhibit identical trends for both N_2 adsorption and desorption. Likewise, Beta-M followed the reversible N_2 physisorption behavior. On the other hand, an H4 hysteresis loop in the P/P_o range 0.5−0.9 is observed in the N_2 physisorption profile for

https://doi.org/10.1021/acsomega.4c07723
ACS Omega 2024, 9, 44760−44769

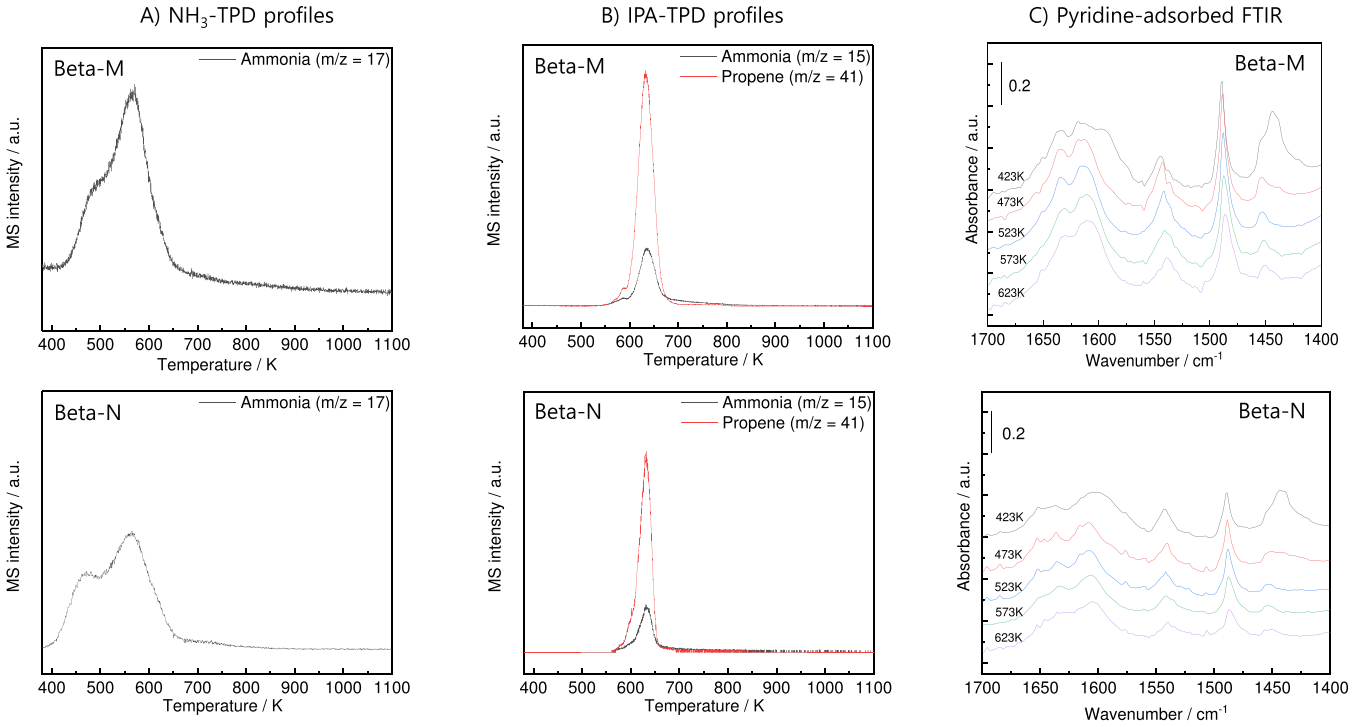

Figure 2. Acidic properties of zeolite Beta catalysts: (A) NH_3-TPD, (B) IPA-TPD, and (C) pyridine-adsorbed FTIR.

Table 1. Physical Properties of Zeolites

		surface area ($m^2 \cdot g^{-1}$)			pore volume ($cm^{-1} \cdot g^{-1}$)			particle size (nm)		acidity (μmol g^{-1})			
catalyst	Si/Al ratio	S_{total}[a]	S_{micro}	S_{meso}	V_{total}	V_{micro}	V_{meso}	TEM	XRD[b]	total acidity[c]	Brønsted acid sites[e]	L/B ratio[f]	Lewis acid sites
Beta-N	12.5	501	300	201	0.22	0.13	0.9	17.4	15.7	713 (LT/HT: 241/472)[d]	468	0.6	280.8
Beta-M	14.0	538	519	19.1	0.28	0.22	0.06	252	152.8	814 (223/591)	615	0.3	184.5

[a] $S_{total} = S_{micro} + S_{meso}$. [b] Scherrer equation $\tau = K\lambda/\beta\cos\theta$. [c] NH_3-TPD. [d] L.T. and H.T. correspond to low (<573 K) and high (>573 K) temperature ranges for NH_3 desorption, respectively. [e] Isopropylamine (IPA)-TPD. [f] Pyridine-FTIR at 473 K.

the Beta-N, indicating the retention of mesopores. The mesoporosity may be explained as the interparticulate mesopore system formed by the agglomerates of the individual zeolite nanocrystals. This phenomenon can be attributed to the presence of nonrigid aggregates of nanosized crystallites.[30] Moreover, as indicated by the pore size distribution curve in Figure 1C, Beta-M only possesses micropores with a diameter of less than 1 nm, whereas Beta-N contains both micropores and mesopores. The mesopores in Beta-N have an average diameter of 2.2 nm, which is consistent with the findings of prior research.[31] Our earlier investigation revealed that Beta-N has the ability to preserve mesopores formed by the agglomeration of secondary particles, namely, interparticulate mesopores.[32] The beneficial effect of smaller particle size of zeolite catalysts on the gasoline-range oil production has been reported by Fu et al.[33] Tarach et al. also observed the formation of mesopores of less than 2.5 nm developed by embryo-ZSM-5 agglomerates.[17]

Figure 2 illustrates the acidic properties of the zeolite Beta catalysts including NH_3-TPD, isopropylamine (IPA)-TPD, and pyridine-adsorbed FTIR profiles. The quantifications of the acidity are also summarized in Table 1. The total acidity obtained by NH_3-TPD shows more acidic sites for Beta-M than Beta-N, with 814 and 713 μmol g^{-1}. In addition, Beta-M is found to have stronger acidic sites than Beta-N of which NH_3 was described at over 573 K (591 vs 472 μmol g^{-1}). The probe molecule IPA is known to decompose to form propylene and ammonia via Hoffmann elimination reaction over Brønsted acid sites (BAS).[34] This reaction thus enables the identification and quantification of the Brønsted acidity. Given the fragmentations of propylene and ammonia characteristic MS peaks at m/z values of 41 and 15, respectively, it is evident that the peak observed at 635 K is a result of the decomposition of IPA on the Brønsted acid sites (BAS). The resulting quantification of the BAS for Beta-M was found higher than that of Beta-N with 615 and 468 μmol g^{-1}, respectively, of which amounts are close to those of strong acid sites obtained in NH_3-TPD. These results can be understood in terms of the difference in crystallinity of the zeolites. It is also known that with the level of crystallinity, the zeolite beta catalyst displayed an enhanced microporosity and acid density.[35] Pyridine-adsorbed FTIR profiles show stronger intensity for Beta-M at 1545 cm^{-1}, assigned to the Brønsted acid sites (BAS), which is in line with the IPA-TPD results. Using the amount of BAS obtained from IPA-TPD and the relative IR peak intensity for those assigned to Brønsted acid sites (BAS) and Lewis acid sites (LAS) at 1540 and 1450 cm^{-1}, respectively,[36] the amount of LAS was estimated as given in

https://doi.org/10.1021/acsomega.4c07723
ACS Omega 2024, 9, 44760−44769

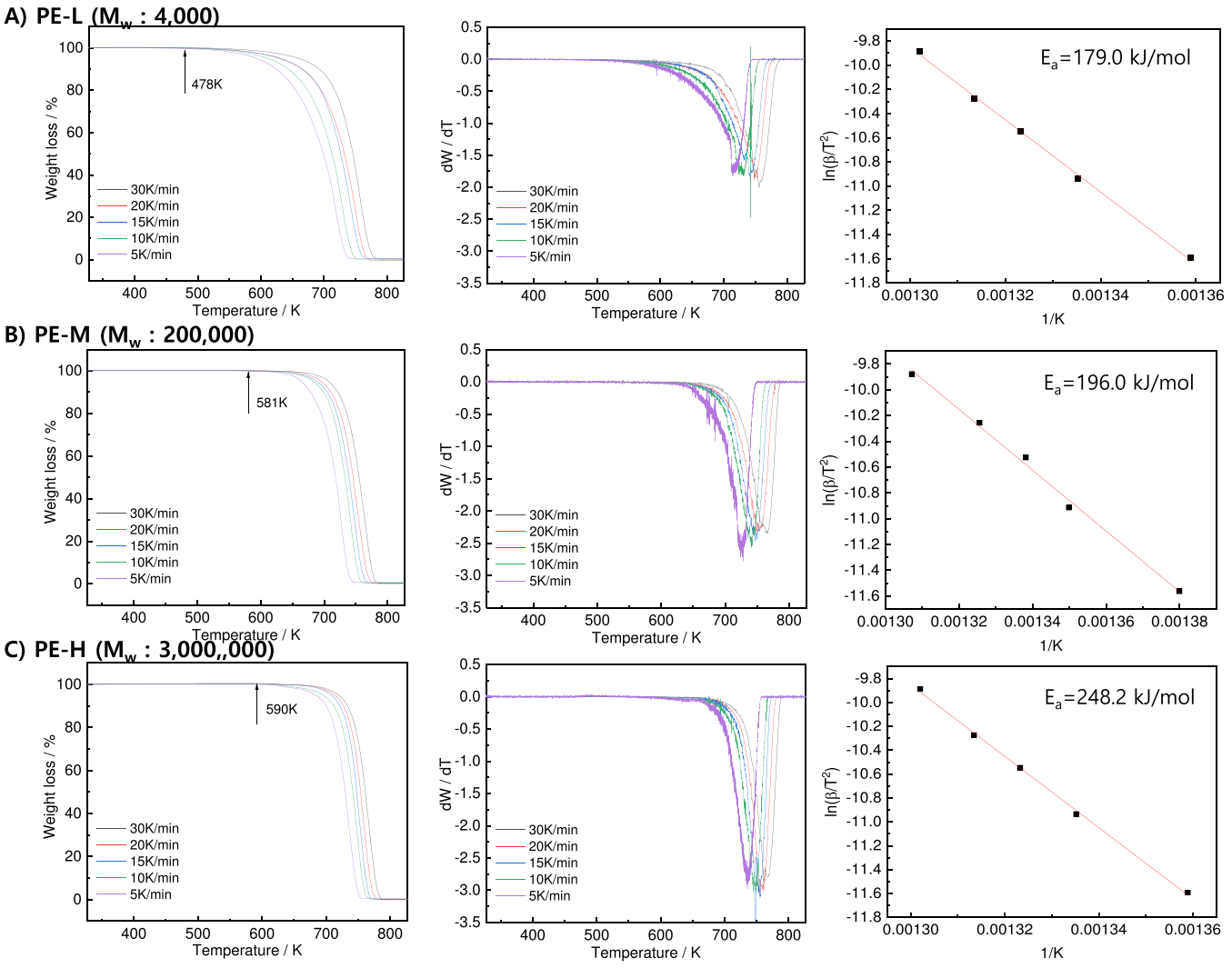

Figure 3. TGA, DTG profiles, and Kissinger plots for (A) PE-L, (B) PE-M, and (C) PE-H.

Table 1. The amounts of Lewis acid sites estimated through pyridine-FTIR and IPA-TPD were observed in a range similar to those of weak acid sites obtained by NH_3-TPD.

3.2. Activation Energy of Catalytic Decomposition of Different Mw PEs. Isothermal thermogravimetric analysis (TGA) using various heating rates has been widely used to obtain kinetic information from the decomposition of polymers and their composites. Garforth et al.[37] have shown that the catalytic degradation of polyolefins may be investigated using thermogravimetric analysis (TGA) as a potential method for screening catalysts, and likewise, USY and SAPO-37 were applied for catalytic decomposition of polymers using TGA.[38,39] In this study, the Kissinger equation was employed to obtain the activation energy of the thermal decomposition of polyethylene in the absence or presence of a catalyst.

$$\ln\left(\frac{\beta}{T_m^2}\right) = -\frac{E_d}{RT_m} + \ln\left(\frac{AR}{E_d}\right) \quad (1)$$

where β is the heating rate (K·min^{-1}), T_m is the temperature (K) at the maximum weight loss rate, E_d is the activation energy (kJ·mol^{-1}), A is the pre-exponential factor, and R is the gas constant.[29]

Figure 3 displays TGA profiles of polyethylenes of low (Mw = 4,000), medium (Mw = 200,000), and high (Mw = 3,000,000) molecular weights (Mw), denoted as PE-L, PE-M, and PE-H, respectively. It is observed that the thermal degradation is initiated at 478, 581, and 590 K for PE-L, PE-M, and PE-H, respectively, indicating that thermal degradation is affected by the molecular weight of the PE, allowing for lighter PE decomposing at a lower temperature. The activation energies for the thermal decompositions of the PE samples were determined using Kissinger plots, as shown in Figure 3B, in which the activation energy for the thermal decomposition follows the order, PE-L, PE-M, and PE-H with the activation energies of 179.0, 196.0, and 248.2 kJ·mol^{-1}, respectively.

Figure 4 displays TGA profiles and Kissinger plots for the decompositions of the medium-molecular-weight PE-M (Mw = 200,000) in the presence of 10 wt % zeolite Beta catalysts. It can be noted that the thermal degradation of PE-M in the presence of zeolite Beta-M and Beta-N is initiated at 473 and 490 K, respectively, which is approximately 100 K lower than in the absence of a catalyst, indicating that the catalytic cracking facilitates the PE decomposition to occur at lower temperatures. The lower initiation temperature (T_i) of thermal decomposition for Beta-M than for Beta-N can be attributed to the higher acidity of Beta-M of which Brønsted acid sites were

https://doi.org/10.1021/acsomega.4c07723
ACS Omega 2024, 9, 44760−44769

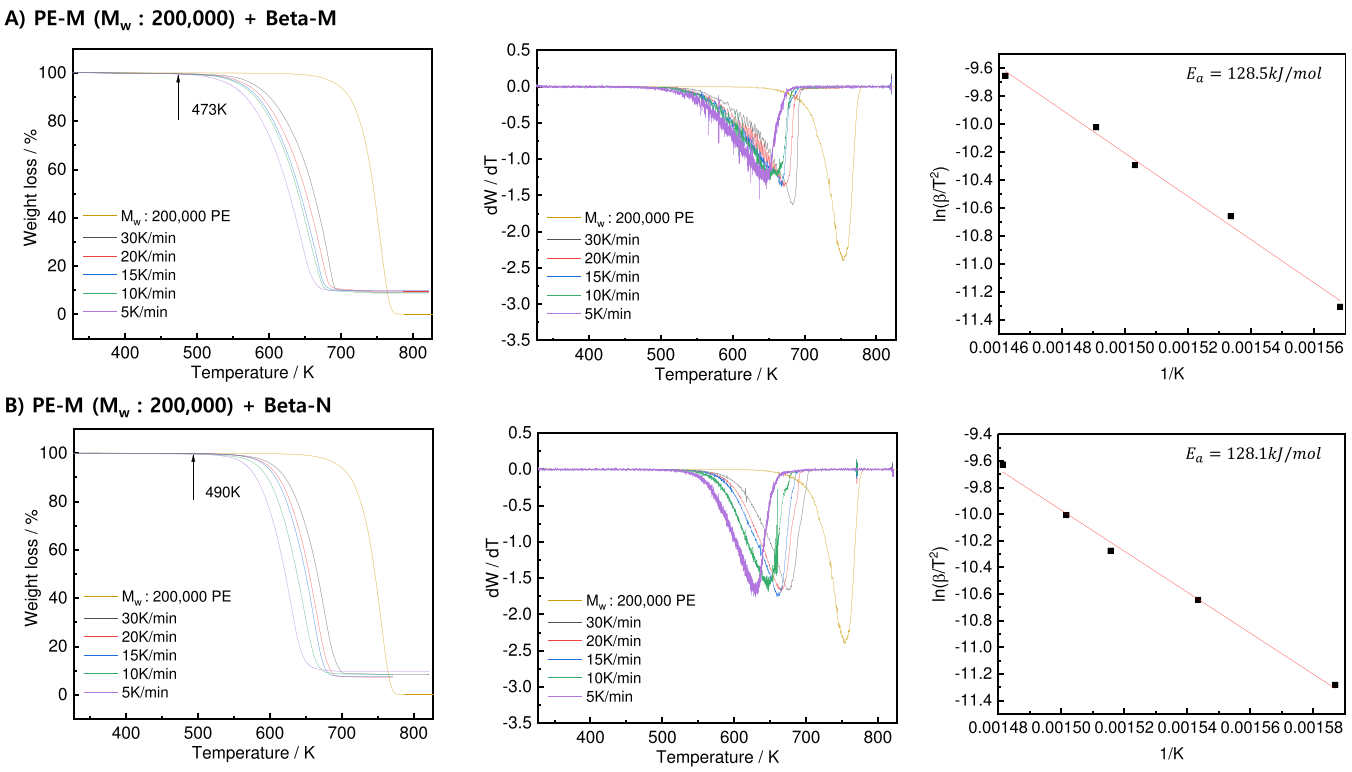

Figure 4. TGA, DTG profiles, and Kissinger plots for (A) PE-M+Beta-M and (B) PE-M+Beta-N.

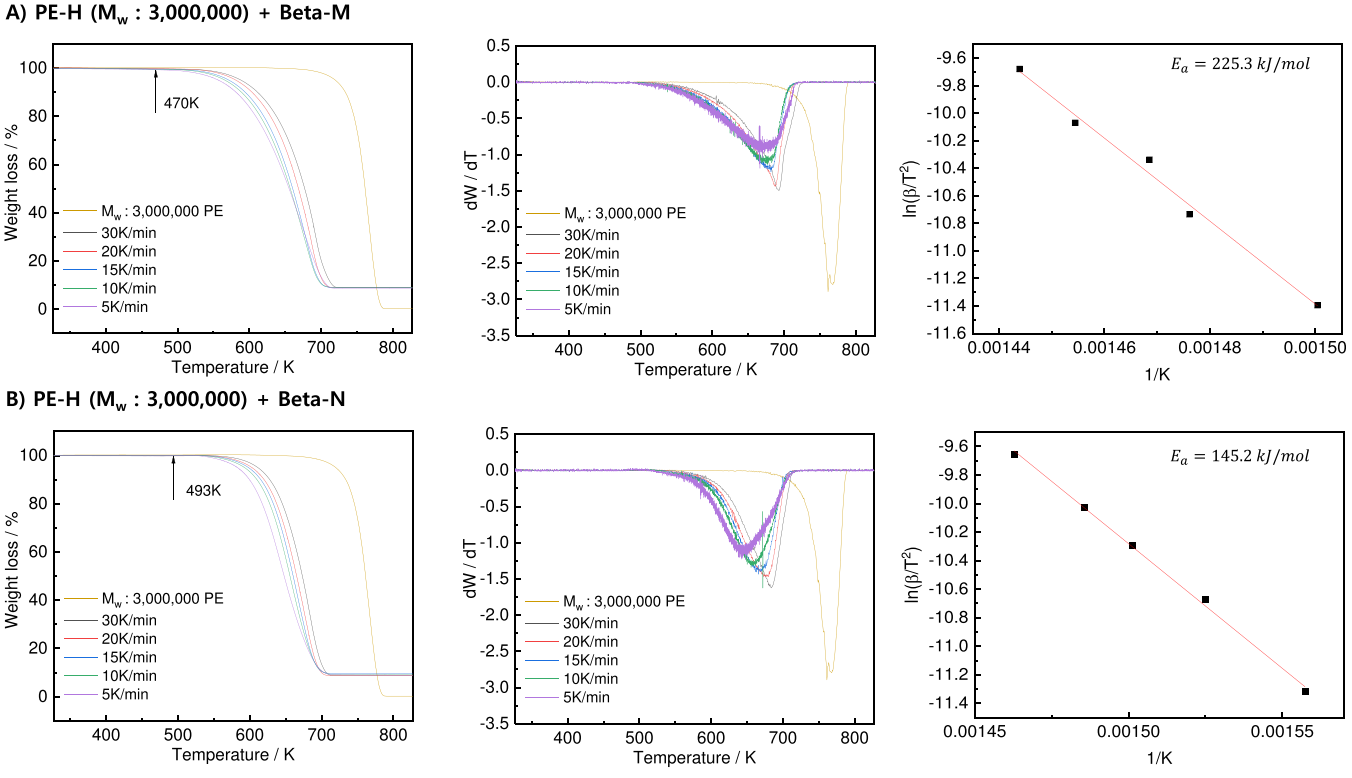

Figure 5. TGA, DTG profiles, and Kissinger plots for (A) PE-H+Beta-M and (B) PE-H+Beta-N.

more abundant on Beta-M than on Beta-N, as given in Figure 2 and Table 2. Nonetheless, compared to the activation energy of the thermal decomposition of PE-M of 196 kJ·mol^{-1}, the activation energies of PE-M in the presence of the catalyst became lower at similar levels around 128 kJ·mol^{-1} for both Beta-M and Beta-N. The observed outcomes can be explained by the difference in the decomposition rate, which can be determined by the temperature at the maximum decomposition rate, T_m. The lower T_m represents the faster decomposition of the PE. As will be depicted in Figure 6,

https://doi.org/10.1021/acsomega.4c07723
ACS Omega 2024, 9, 44760−44769

Table 2. Thermal Decomposition Properties of PE in the Absence or Presence of the Catalyst in TGA

		T_m[b]/K					
sample	T_i[a]/K	at 5 K/min	at 10 K/min	at 15 K/min	at 20 K/min	30 K/min	E_a[c]/kJ·mol^{-1}
PE-L	478	714	731	742	748	756	179.0
PE-M	581	725	741	747	753	765	196.0
PE-H	590	736	749	756	761	768	248.2
PE-M+Beta-M	473	638	652	665	671	684	128.5
PE-M+Beta-N	490	630	647	660	666	675	128.1
PE-H+Beta-M	470	666	677	681	687	692	225.3
PE-H+Beta-N	493	642	656	666	673	684	145.3

[a]Temperature at 1% weight loss. [b]Temperature at the maximum decomposition rate collected at DTG. [c]Obtained by Kissinger plots.

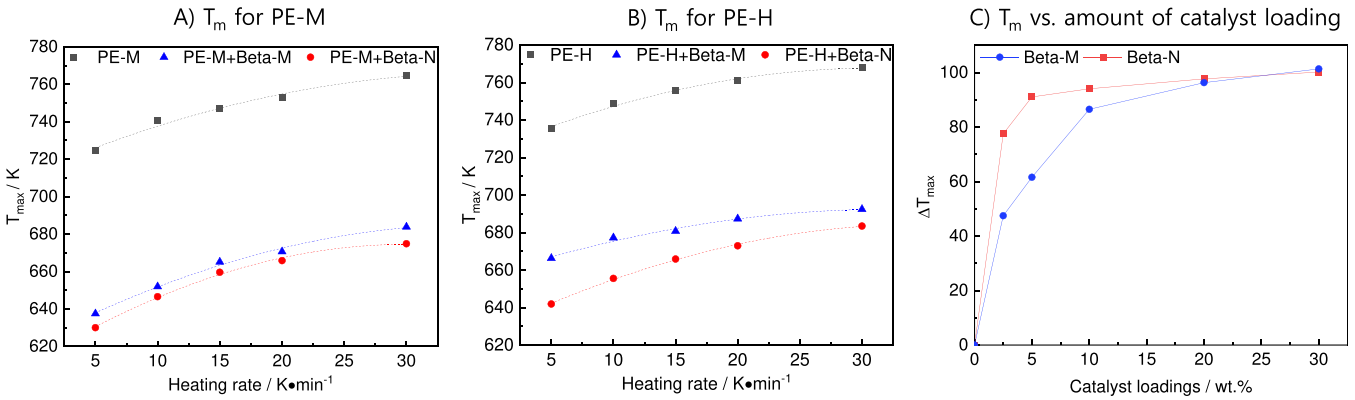

Figure 6. Effect of different heating rates and amounts of catalyst loading on PE decomposition in TGA.

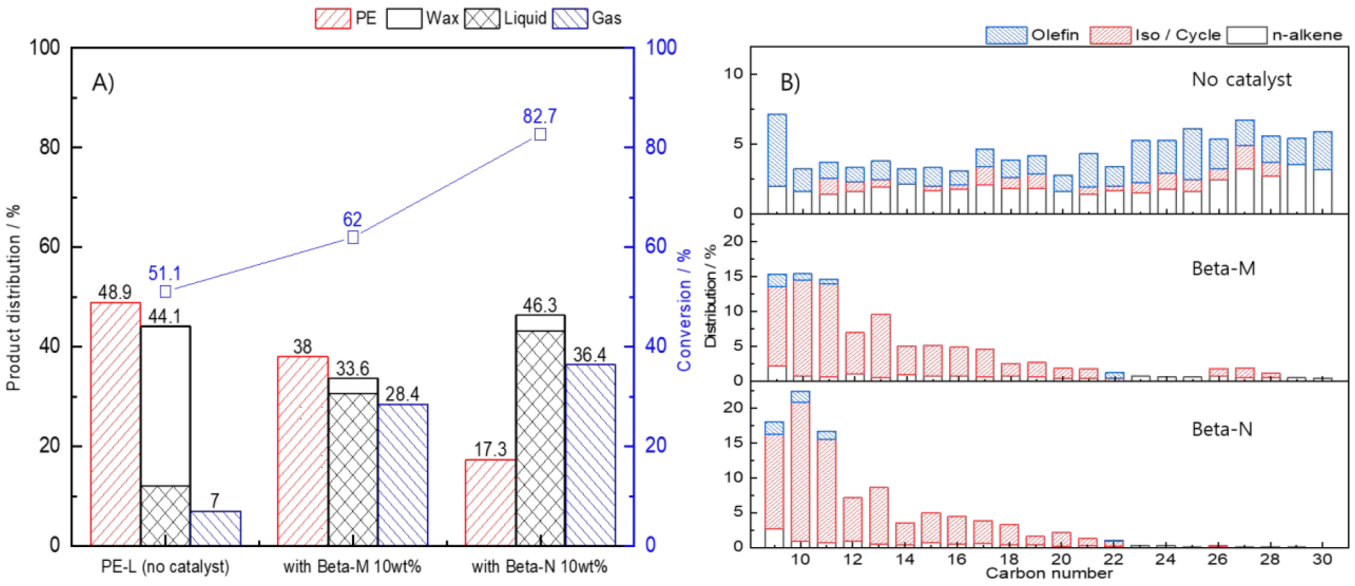

Figure 7. Comparison of thermal and catalytic cracking of PE-L: (A) product distributions by phase and (B) liquid product distributions by carbon number.

T_m profiles collected at different heating rates were found to be even lower for Beta-N than Beta-M, indicating that the decomposition of PE-M over Beta-N occurs faster than over Beta-M.

The TGA profiles and Kissinger plots for the decompositions of the high-molecular-weight PE-H (Mw = 3,000,000) in the presence of 10 wt % zeolite Beta catalysts are depicted in Figure 5. It can be noted that the thermal degradation of PE-H in the presence of zeolite Beta-M and Beta-N is initiated at 470 and 493 K, respectively, which is approximately 90K lower than in the absence of a catalyst (581 K), again, further supporting that the catalytic cracking promotes PE decomposition. The lower initiation temperature (T_i) of thermal decomposition for Beta-M than for Beta-N is also observed, as in the case of PE-M. On the other hand, it is worth mentioning that the activation energies of the PE-H in the presence of the catalysts became lower, particularly for Beta-N at 145.3 kJ·mol^{-1}. For Beta-M, however, the activation energy of the PE-H was 225.3 kJ·mol^{-1}, which is much more than that of Beta-N. These results suggest that the morphology

https://doi.org/10.1021/acsomega.4c07723
ACS Omega 2024, 9, 44760−44769

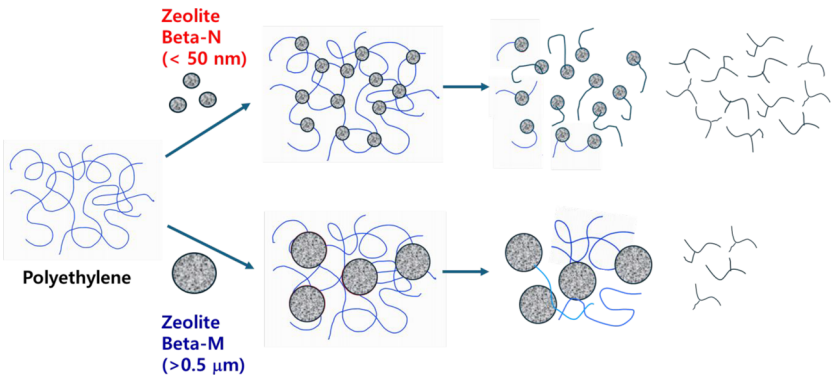

Figure 8. Schematic of catalytic cracking of low-density polyethylene (LDPE) using zeolite Beta with different particle sizes.

effect of the zeolite Beta is more influential on the high Mw PE, with nanoscaled Beta-N having better activity than Beta-M. Compared to E_a in the absence of a catalyst, 248.5 kJ/mol, the PE-M decomposition with Beta-M exhibits a slight decrease in E_a of 225.3 kJ/mol, implying that the contribution of Beta-M is not influential. These findings suggest that micrometer-sized zeolites show a lower catalytic activity for high Mw polymers. In other words, it can be inferred that the catalytic cracking of high Mw is more challenging due to the mass transport limitation, leading to dependence upon the types of catalysts, more specifically, the morphologies of zeolite catalysts.

Figure 6 presents T_m profiles with respect to the increase in the heating rate in the TGA analysis and the effect of the catalyst loadings. It is obvious that the role of the catalyst is crucial in the temperature reduction for PE decomposition, leading to a significant difference of around 100 K in the T_m when comparing the absence and presence of catalysts for the decomposition of PE-M. Again, Beta-N shows a lower T_m profile than Beta-M for the decomposition of PE-M, supporting a superior effect of smaller zeolite particles. Furthermore, the morphological effect is more significant for the high Mw PE-H, with the difference between T_m of Beta-M and Beta-N being larger than the case for PE-M. These results suggest that the nanoscaled zeolite Beta provides better accessibility toward PE-H than micron-scaled Beta-M. The morphological effect is more obvious when the amount of catalyst loadings on the decomposition of PE is compared for Beta-M and Beta-N. As shown in the effect of catalyst loadings on the ΔT_m for those obtained in the absence and presence of Beta-M or Beta-N in Figure 6C, the smaller particle Beta-N is found to require 5% loading to reach the maximum catalytic effect, while the larger particle Beta-M needs over 10%, indicating that the smaller Beta-N is more efficient than the larger particle Beta-M in the decomposition of the PE. Tarach et al. also reported similar results that nanoscaled embryo ZSM-5 with a high external surface area exhibited better activity in polypropylene decomposition than a larger particle ZSM-5.[33]

3.3. Catalytic Cracking of PE over Two Types of Zeolite Beta. Figure 7 compares product distributions of the cracking of PE-L conducted in an autoclave batch reactor at 623 K for 2 h in the absence or presence of catalysts. It is observed that the PE thermal cracking without a catalyst shows a lower PE conversion of 51%, with the predominant generation of wax as the main product. In addition, the liquid product is composed of a wide range of hydrocarbons with a combination of *n*-alkanes and 1-alkenes.[40] On the other hand, the zeolite Beta catalysts showed a higher PE conversion in both cases and readily cracked the PE into smaller molecules containing less than 20 carbon atoms (Figure S2 and Table S1). It can be noted that Beta-N exhibits better activity than Beta-M with the formation of iso/cycloparaffin as the primary products in the liquid. The catalytic cracking can be understood to follow protolytic cracking, where long-chain hydrocarbons are adsorbed onto Brønsted acid sites, protonated, and transformed into carbonium ions. These carbonium ions are then broken to form alkane and carbenium ions.[41] Carbenium ions undergo intramolecular hydrogen transfer to create isomerized carbenium ions. Afterward, they undergo further protolytic cracking and β-scissions, resulting in the production of smaller carbenium ions and n- or isomeric hydrocarbons.[42,43] The production of these products is influenced by the structure and acidity of the zeolite catalysts. According to this, polyolefin molecules can undergo successive protolytic cracking, resulting in the production of low-molecular-weight hydrocarbons. It is important to ensure that the sample used in a TGA experiment should be sufficiently small so that the effects of heat and mass transfer can be ignored. This ensures that any degradation of a polymer is mostly controlled by its kinetics.[44] This observation is applicable to both low- and medium-molecular-weight polyethylene (PE) samples, as they exhibited identical activation energies (E_a) for the degradation reactions of Beta-M and Beta-N in the presence of a medium-molecular-weight PE-M (Mw = 200,000) in the thermogravimetric analysis (TGA). This suggests that at low concentrations of PE and a catalyst, the degradation process is mostly controlled by the kinetics. However, in the case of PE cracking in an actual reactor, when a significant quantity of PE and a catalyst is employed, the restrictions imposed by mass and heat transmissions should have a significant impact. Although the high-pressure reaction circumstances can reduce the limitations of heat and mass transfer, the difference in catalytic performance between Beta-M and Beta-N was dramatic, with the smaller particle Beta-N being more active than the larger particle Beta-M. Given that they showed a similar E_a in TGA analysis for the PE-M decomposition, the difference in the real catalytic performance in the PE cracking is remarkable. These results thus demonstrate that high-molecular-weight molecules like polymers lead to transfer limitations, particularly in the real processes, requiring more catalysts than expected due to the limitations. Therefore, more care should be taken for the catalyst design to achieve better dispersion in the polymer melt and to provide better accessibility toward active centers.

https://doi.org/10.1021/acsomega.4c07723
ACS Omega 2024, 9, 44760−44769

Figure 8 illustrates the reaction schematic for catalytic PE cracking in the presence of two types of zeolite Beta catalysts. The catalytic cracking can be understood to follow protolytic cracking, where PE chains are adsorbed onto Brønsted acid sites and undergo protonation to form carbonium ions. The carbonium ions are then converted to alkane and carbenium ions. A part of the produced alkanes can be adsorbed on Brønsted acid sites to undergo subsequent protolytic cracking. Carbenium ions may undergo intramolecular hydrogen transfer to create isomerized carbenium ions, followed by β-scissions, resulting in the production of smaller carbenium ions and n- or isomeric hydrocarbons. The smaller zeolite Beta exhibits a higher dispersion, penetrating more effectively into the PE networks, while the larger Beta shows a poor dispersion, leading to a low PE conversion in catalytic PE cracking. Overall, it can be suggested that a nanoscaled zeolite Beta with a moderate acidity and interparticulate mesopores, leading to high dispersion in PE melt and better accessibility for acid sites, plays key roles in overcoming the transfer limitations and enhancing the catalytic activity to facilitate the PE cracking to produce valuable naphtha and middle distillates.

CONCLUSIONS

The catalytic degradation of three separate LDPE samples with low, medium, and high molecular weights of 4000, 200,000, and 3,000,000, respectively, was studied using two types of zeolite Beta catalysts with particle sizes in the nano or micrometer scale (Beta-N or Beta-M). Thermal gravity analysis with catalysts showed that nanosized Beta-N had a slightly higher temperature at which decomposition starts (T_i) compared to Beta-M for all types of polyethylene (PE). This is because Beta-N has a moderate level of acidity. However, Beta-N had a lower temperature at which decomposition occurs at the fastest rate (T_m), resulting in a lower activation energy compared to Beta-M for catalytic decomposition of PE. This difference was especially significant for high-molecular-weight PE (225.3 vs 145.3 kJ/mol). In addition, Beta-N demonstrated superior performance in the cracking of PE-L in a real batch reactor. Specifically, Beta-N achieved an 82.7% conversion rate, whereas Beta-M only achieved 62.0%. The characterizations revealed that Beta-N has abundant interparticulate mesopores, which allows for improved dispersion in polymers and increased accessibility to acid sites. As a result, Beta-N exhibits exceptional activity in the cracking of polyethylene (PE), showing promise as a catalyst for converting polyolefins into valuable naphtha and middle distillates through the process of cracking.

ASSOCIATED CONTENT

Supporting Information

The Supporting Information is available free of charge at https://pubs.acs.org/doi/10.1021/acsomega.4c07723.

Schematic of autoclave batch reactor system for catalytic PE cracking (Figure S1), GC/FID chromatograms for the PE cracking products in the absence or presence of catalysts (Figure S2), derivation of Kissinger equation (Figure S3), and GC/FID peak assignments obtained by MS analysis (Table S1) (PDF)

AUTHOR INFORMATION

Corresponding Author

Yong-Kul Lee − *Laboratory of Advanced Catalysis for Energy and Environment, Department of Chemical Engineering, Dankook University, Yongin 16890, South Korea;* orcid.org/0000-0001-6800-556X; Email: yolee@dankook.ac.kr

Authors

Jeonghwan Seo − *Laboratory of Advanced Catalysis for Energy and Environment, Department of Chemical Engineering, Dankook University, Yongin 16890, South Korea*

Daeun Kim − *Laboratory of Advanced Catalysis for Energy and Environment, Department of Chemical Engineering, Dankook University, Yongin 16890, South Korea*

Complete contact information is available at: https://pubs.acs.org/10.1021/acsomega.4c07723

Notes

The authors declare no competing financial interest.

ACKNOWLEDGMENTS

The authors acknowledge financial support from the National Research Foundation of Korea (NRF-2022R1A4A5033554 and NRF-2022R1A2C2093257).

REFERENCES

(1) Palos, R.; Gutiérrez, A.; Vela, F. J.; Olazar, M.; Arandes, J. M.; Bilbao, J. Waste Refinery: The Valorization of Waste Plastics and End-of-Life Tires in Refinery Units. A Review. *Energy Fuels* **2021**, *35*, 3529−3557.

(2) Al-Salem, S. M.; Lettieri, P.; Baeyens, J. Recycling and Recovery Routes of Plastic Solid Waste (PSW): A Review. *J. Waste Manag.* **2009**, *29*, 2625−2643.

(3) Zhang, F.; Zhao, Y.; Wang, D.; Yan, M.; Zhang, J.; Zhang, P.; Ding, T.; Chen, L.; Chen, C. Current Technologies for Plastic Waste Treatment: A Review. *J. Clean. Prod.* **2021**, *282*, No. 124523.

(4) Soni, V. K.; Singh, G.; Vijayan, B. K.; Chopra, A.; Kapur, G. S.; Ramakumar, S. S. V. Thermochemical Recycling of Waste Plastics by Pyrolysis: A Review. *Energy Fuels* **2021**, *35*, 12763−12808.

(5) Kaminsky, W.; Mennerich, C.; Zhang, Z. Feedstock recycling of synthetic and natural rubber by pyrolysis in a fluidized bed. *J. Anal. Appl. Pyrolysis* **2009**, *85*, 334−337.

(6) Zhao, Y.; Rettner, E. M.; Harry, K. L.; Hu, Z.; Miscall, J.; Rorrer, N. A.; Miyake, G. M. Chemically recyclable polyolefin-like multiblock polymers. *Science* **2023**, *382*, 310−314.

(7) Akhtar, M. N.; Riaz, S.; Ahmad, N.; Jaseer, E. A. Pioneering Aromatic Generation from Plastic Waste via Catalytic Thermolysis: A Minireview. *Energy Fuels* **2024**, *38*, 11363−11390.

(8) Vollmer, I.; Jenks, M. J. F.; Roelands, M. C. P.; White, R. J.; van Harmelen, T.; de Wild, P.; van der Laan, G. P.; Meirer, F.; Keurentjes, J. T. F.; Weckhuysen, B. M. Beyond Mechanical Recycling: Giving New Life to Plastic Waste. *Angew. Chem.* **2020**, *59*, 15402−15423.

(9) Li, H. Q.; Wu, J. Y.; Jiang, Z.; Ma, J. Z.; Zavala, V. M.; Landis, C. R.; Mavrikakis, M.; Huber, G. W. Hydroformylation of pyrolysis oils to aldehydes and alcohols from polyolefin waste. *Science* **2023**, *381*, 660−666.

(10) Dong, Z.; Chen, W.; Xu, K.; Liu, Y.; Wu, J.; Zhang, F. Understanding the Structure−Activity Relationships in Catalytic Conversion of Polyolefin Plastics by Zeolite-Based Catalysts: A Critical Review. *ACS Catal.* **2022**, *12*, 14882−14901.

(11) Onwudili, J. A.; Insura, N.; Williams, P. T. Composition of products from the pyrolysis of polyethylene and polystyrene in a closed batch reactor: Effects of temperature and residence time. *J. Anal. Appl. Pyrolysis* **2009**, *86*, 293−303.

(12) Vollmer, I.; Jenks, M. J. F.; Mayorga González, R.; Meirer, F.; Weckhuysen, B. M. Plastic Waste Conversion over a Refinery Waste Catalyst. *Angew. Chem.* **2021**, *60*, 16101−16108.
(13) Aguado, J.; Sotelo, J. L.; Serrano, D. P.; Calles, J. A.; Escola, J. M. Catalytic Conversion of Polyolefins into Liquid Fuels over MCM-41: Comparison with ZSM-5 and Amorphous SiO_2-Al_2O_3. *Energy Fuels* **1997**, *11*, 1225−1231.
(14) Shamzhy, M.; Opanasenko, M.; Concepcion, P.; Martinez, A. New trends in tailoring active sites in zeolite-based catalysts. *Chem. Soc. Rev.* **2019**, *48*, 1095−1149.
(15) Awala, H.; Gilson, J. P.; Retoux, R.; Boullay, P.; Goupil, J. M.; Valtchev, V.; Mintova, S. Template-free nanosized faujasite-type zeolites. *Nat. Mater.* **2015**, *14*, 447−451.
(16) Fan, L.; Liu, L.; Xiao, Z.; Su, Z.; Huang, P.; Peng, H.; Lv, S.; Jiang, H.; Ruan, R.; Chen, P.; Zhou, W. Comparative study of continuous-stirred and batch microwave pyrolysis of linear low-density polyethylene in the presence/absence of HZSM-5. *Energy* **2021**, *228*, No. 120612.
(17) Tarach, K. A.; Akouche, M.; Pyra, K.; Valtchev, V.; Jajko, G.; Gilson, J. P.; Góra-Marek, K. Polypropylene cracking on embryonic and ZSM-5 catalysts - An operando study. *Appl. Catal., B* **2023**, *324*, No. 122871.
(18) Haw, K. G.; Gilson, J. P.; Nesterenko, N.; Akouche, M.; El Siblani, H.; Goupil, J. M.; Rigaud, B.; Minoux, D.; Dath, J. P.; Valtchev, V. Supported embryonic zeolites and their use to process bulky molecules. *ACS Catal.* **2018**, *8*, 8199−8212.
(19) Akouche, M.; Gilson, J. P.; Nesterenko, N.; Moldovan, S.; Chateigner, D.; Siblani, H. E.; Minoux, D.; Dath, J. P.; Valtchev, V. Synthesis of embryonic zeolites with controlled physicochemical properties. *Chem. Mater.* **2020**, *32*, 2123−2132.
(20) Marcilla, A.; Gómez-Siurana, A.; Valdés, F. Catalytic cracking of low-density polyethylene over H-Beta and HZSM-5 zeolites: Influence of the external surface. Kinetic model. *Polym. Degrad. Stab.* **2007**, *92*, 197−204.
(21) Aguado, J.; Serrano, D. P.; Escola, J. M.; Garagorri, E.; Fernández, J. A. Catalytic conversion of polyolefins into fuels over zeolite beta. *Polym. Degrad. Stab.* **2000**, *69*, 11−16.
(22) Kokuryo, S.; Tamura, K.; Tsubota, S.; Miyake, K.; Uchida, Y.; Mizusawa, A.; Kubo, T.; Nishiyama, N. Coking Reduction of Cr-loaded Beta Zeolite during Polymer Cracking: Hydrocracking of Aromatics by Synergistic Effect of Cr^{6+} and Zeolitic Acid Sites. *ChemCatChem.* **2023**, *15*, No. e202300461.
(23) Kokuryo, S.; Miyake, K.; Uchida, Y.; Mizusawa, A.; Kubo, T.; Nishiyama, N. Defect engineering to boost catalytic activity of Beta zeolite on low-density polyethylene cracking. *Mater. Today Sustain.* **2022**, *17*, No. 100098.
(24) Bikbaeva, V.; Nesterenko, N.; Konnov, S.; Nguyen, T. S.; Gilson, J. P.; Valtchev, V. A low carbon route to ethylene: Ethane oxidative dehydrogenation with CO_2 on embryonic zeolite supported Mo-carbide catalyst. *Appl. Catal., B* **2023**, *320*, No. 122011.
(25) Alonso-Doncel, M.; Peral, A.; Ochoa-Hernández, C.; Sanz, R.; Serrano, D. P. Tracking the evolution of embryonic zeolites into hierarchical ZSM-5. *J. Mater. Chem.* **2021**, *A 9*, 13570−13587.
(26) Qiu, B.; Lu, W. D.; Gao, X. Q.; Sheng, J.; Ji, M.; Wang, D.; Lu, A. H. Boosting the propylene selectivity over embryonic borosilicate zeolite catalyst for oxidative dehydrogenation of propane. *J. Catal.* **2023**, *417*, 14−21.
(27) Wang, L.; Zhu, D.; Wang, J.; Cui, W.; Han, J.; Li, B.; Fan, D.; Tian, P.; Liu, Z. Embryonic zeolite-assisted synthesis of SSZ-13 with superior efficiency and their excellent catalytic performance. *J. Mater. Chem.* **2021**, *A 9*, 15238−15245.
(28) Liu, Y.; Dai, W.; Zheng, J.; Du, Y.; Wang, Q.; Hedin, N.; Qin, B.; Li, R. Selective and Controllable Cracking of Polyethylene Waste by Beta Zeolites with Different Mesoporosity and Crystallinity. *Adv. Sci.* **2024**, *11*, No. 2404426.
(29) Kissinger, H. E. Reaction kinetics in differential thermal analysis. *Anal. Chem.* **1957**, *29*, 1702−1706.
(30) Sangwichien, C.; Aranovich, G.; Donohue, M. Density functional theory predictions of adsorption isotherms with hysteresis loops. *Colloids Surf. A: Physicochem. Eng. Aspects* **2002**, *206*, 313−320.
(31) van Laak, A. N.; Sagala, S. L.; Zecevic, J.; Friedrich, H.; de Jongh, P. E.; de Jong, K. P. Mesoporous mordenites obtained by sequential acid and alkaline treatments- Catalysts for cumene production with enhanced accessibility. *J. Catal.* **2010**, *276*, 170−180.
(32) Kim, Y.-S.; Cho, K.-S.; Lee, Y.-K. Morphology effect of b-zeolite supports for Ni2P catalysts on the hydrocracking of polycyclic aromatic hydrocarbons to benzene, toluene, and xylene. *J. Catal.* **2017**, *351*, 67−78.
(33) Fu, T.; Zhou, H.; Li, Z. Effect of Particle Morphology for ZSM-5 Zeolite on the Catalytic Conversion of Methanol to Gasoline-Range Hydrocarbons. *Catal. Lett.* **2016**, *146*, 1973−1983.
(34) Pereira, C.; Gorte, R. J. Method for distinguishing Brønsted-acid sites in mixtures of H-ZSM-5, H-Y and silica-alumina. *Appl. Catal., A* **1992**, *90*, 145−157.
(35) Duan, J. D.; Chen, W.; Wang, C. T.; Wang, L.; Liu, Z. Q.; Yi, X. F.; Fang, W.; Wang, H.; Wei, H.; Xu, S. D.; Yang, Y. W.; Yang, Q. W.; Bao, Z. B.; Zhang, G.; Ren, Q. L.; Zhou, H.; Qin, X. D.; Zheng, A. M.; Xiao, F. S. Coking-Resistant Polyethylene Upcycling Modulated by Zeolite Micropore Diffusion. *J. Am. Chem. Soc.* **2022**, *144*, 14269−14277.
(36) Coudurier, G.; Naccache, C.; Vedrine, J. C. Uses of i.r. spectroscopy in identifying ZSM zeolite structure. *J. Chem. Soc., Chem. Commun.* **1982**, 1413−1415.
(37) Garforth, A.; Fiddy, S.; Lin, Y.-H.; Ghanbari-Siakhali, A.; Sharratt, P. N.; Dwyer, J. Catalytic degradation of high density polyethylene: an evaluation of mesoporous and microporous catalysts using thermal analysis. *Thermochim. Acta* **1997**, *294*, 65−69.
(38) Gobin, K.; Manos, G. Thermogravimetric study of polymer catalytic degradation over microporous materials. *Polym. Degrad. Stab.* **2004**, *26*, 225−231.
(39) Fernandes, G. J. T.; Fernandes, V. J.; Araujo, A. S. Catalytic degradation of polyethylene over SAPO-37 molecular sieve. *Catal. Today* **2002**, *75*, 233−238.
(40) Tarach, K. A.; Akouche, M.; Pyra, K.; Valtchev, V.; Jajko, G.; Gilson, J.-P.; Góra-Marek, K. GC-MS of polyethylene and polypropylene thermal cracking products. *Pet. Coal* **2006**, *48*, 1−14.
(41) Corma, A.; Orchillés, A. V. Current views on the mechanism of catalytic cracking. *Microporous Mesoporous Mater.* **2000**, *35−36*, 21−30.
(42) Weitkamp, J. Catalytic Hydrocracking Mechanisms and Versatility of the Process. *ChemCatChem.* **2012**, *4*, 292−306.
(43) Corma, A.; Planelles, J.; Sanchez-Marin, J.; Tomas, F. The Role of Different Types of Acid Site in the Cracking of Alkanes on Zeolite Catalysts. *J. Catal.* **1985**, *93*, 30−37.
(44) Richter, F.; Rein, G. The Role of Heat Transfer Limitations in Polymer Pyrolysis at the Microscale. *Front. Mech. Eng.* **2018**, *4*, 18.

https://doi.org/10.1021/acsomega.4c07723
ACS Omega 2024, 9, 44760−44769